

# A 3–10-GHz GaN-Based Flip-Chip Integrated Broad-Band Power Amplifier

Jane J. Xu, Stacia Keller, Gia Parish, Sten Heikman, Umesh K. Mishra, *Fellow, IEEE*, and Robert A. York, *Senior Member, IEEE*

**Abstract**—In this paper, we report the latest progress of a GaN-based broad-band power amplifier using AlGaIn/GaN high electron mobility transistors (HEMTs), grown on sapphire substrates, as the active devices. The devices were flip-chip integrated onto the aluminum nitride circuit board for thermal management and electric connection. The circuit topology used novel *LCR*-matching networks in a four-way binary-Wilkinson combiner structure. Using devices with 0.7- $\mu\text{m}$  gate length and 4-mm gate width, a small-signal gain of 7 dB was obtained with 3–10-GHz bandwidth. Output power of 8 W (continuous wave) at 9.5 GHz with about 20% power-added efficiency was achieved when biased at 24 V, which is the highest output power for a power amplifier using GaN-HEMTs-on-sapphire.

**Index Terms**—Broad-band, flip-chip bonding, GaN high electron mobility transistors (HEMTs), power amplifier.

## I. INTRODUCTION

GaN high electron mobility transistors (HEMTs) have enormous potential for realizing high-power solid-state amplifiers at microwave frequencies. This is due to their characteristics of wide bandgap materials such as high breakdown field, high electron saturation velocity, and high operating temperature. GaN epitaxial layers can be grown on either SiC or single-crystal sapphire ( $\text{Al}_2\text{O}_3$ ) substrates. Sapphire has the advantage of lower cost and availability in larger wafer size than SiC, but it is a poor thermal conductor. GaN HEMTs on SiC have achieved a power density of 6.9–9.2 W/mm [1], [2], while GaN HEMTs on sapphire have demonstrated 6.6 W/mm [3]. The difference is believed to be due to the higher thermal conductivity of SiC ( $\sigma = 450$  W/mK) over sapphire ( $\sigma = 30$  W/mK). However, by paying close attention to thermal management, GaN-HEMT-on-sapphire can still have competitive performance. In particular, adequate thermal management can be achieved through flip-chip bonding of the device onto a thermally conductive, electrically insulating substrate, such as ceramic aluminum nitride (AlN) ( $\sigma = 180$  W/mK), which also hosts the matching networks and combiner networks. Using this technique, we have achieved record-high single-device results of 4.4 W output power [continuous wave (CW)] with a 1-mm-wide GaN HEMT on sapphire. In this paper, we present the results of an ongoing effort at the University of California, Santa Barbara (UCSB), to implement high-power broad-band

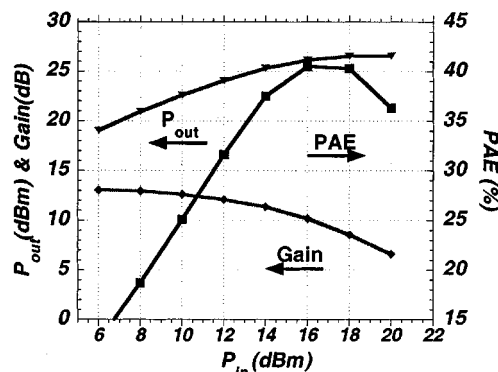


Fig. 1. RF characteristic of a 100- $\mu\text{m}$  device. ( $P_{out} = 4.6$  W/mm, PAE = 40%,  $f = 8$  GHz, biased at  $V_{ds} = 24$  V,  $I_{ds} = 20$  mA, class AB mode).

microwave amplifiers using such a flip-chip mounting GaN large-periphery power device “baseline” process.

## II. GaN POWER DEVICE TECHNOLOGY

Recent progress in material quality and device fabrication technique resulted in much improved GaN/AlGaIn HEMTs on sapphire substrate grown by metal organic chemical vapor deposition (MOCVD) at UCSB. We are able to achieve up to 4.6 W/mm power density with 40% power-added efficiency (PAE) at 8 GHz (Fig. 1). However, the gate peripheries corresponding to these results are on the order of 100  $\mu\text{m}$ . The total amount of produced power is too small to be significantly affected by the poor thermal properties of the sapphire substrate. For GaAs-based large-periphery power devices, heat removal is typically done through backside heat sink and wafer thinning. However, for GaN devices, both techniques are still premature due to the lack of proper etching methods. We circumvent the problem by developing the flip-chip mounting technology with AlN substrate as the heat sink as well as the circuit carrier. As a result, we are able to fabricate GaN HEMTs on sapphire at much lower cost, having competitive performance as GaN-grown-on-SiC without a compromise in thermal management. Also, this technique is scalable to larger devices (1, 2, and 4 mm have been tested) with proper design of the multifinger layout pattern. Table I lists the dc and radio-frequency (RF) performance of the devices with different sizes. RF measurement for the 1-mm device was performed at 8 GHz and for the 2-mm device at 4 GHz. All the power data were obtained under CW operation. Due to the limitation of the load-pull system, the RF performance of the 4-mm device cannot be obtained.

Manuscript received March 2, 2000; revised August 24, 2000. This work was supported by the ONR/MURI program under Contract N000 14-96-1-1215.

The authors are with the Department of Electrical and Computer Engineering, University of California at Santa Barbara, Santa Barbara, CA 93117 USA.

Publisher Item Identifier S 0018-9480(00)10791-4.

TABLE I  
DC AND RF PERFORMANCES OF THE FLIP-CHIPPED LARGE  
GATE-PERIPHERY DEVICES

Device size	$I_{\max}/DC$ (mA)	Gain (dB)	Power (Watt)
1mm*	800 ~ 900	10	4.4
2mm**	1500 ~ 1800	13	6.4
4mm	3000 ~ 3400	N/A	N/A

\*: RF measurement was performed at 8 GHz.

\*\* : RF measurement was performed at 4 GHz.

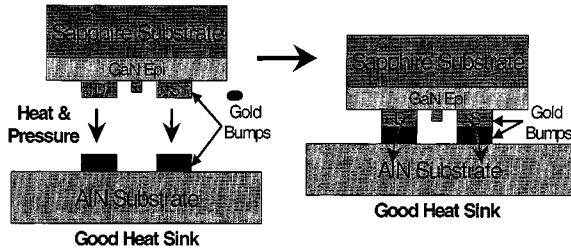


Fig. 2. The procedure of flip-chip bonding technique.

Fig. 2 describes the procedure of the flip-chip bonding. First, we fabricated thick gold bonding bumps on both the GaN chip and the AlN substrate. A flip-chip bonder was then used to align the GaN device to the AlN circuit board with a coplanar waveguide (CPW) lines structure prefabricated to avoid backside grounding. The proper amount of pressure and heat was then applied to bond them together. Other advantages of the flip-chip mounting include 1) the reduced parasitic inductance compared to the conventional wire bonding connection and 2) more cost-effective use of the GaN material with all the passive components built on an inexpensive AlN circuit board.

Fig. 3 shows the picture of a 1-mm-wide device before and after the flip-chip bonding. An interdigital pattern layout was chosen with gate and drain all connected while source pads were disconnected. Since it is not trivial to bond all the gold bumps firmly at the same time, careful design of device layout was needed such as reasonable bonding chip size, pad size and shape, pad alignment tolerance, etc., to facilitate the bonding process. The enlarged source and drain pads were used to reduce the thermal resistance of the device; the connection of the source pads was made on the AlN substrate to avoid the use of air bridges. The tradeoff is the increased pad parasitic capacitances, which must be taken into account during the circuit design.

Fig. 4 is the measured power performance of a 1-mm-wide device using an ATN LP1 loadpull system. With only fundamental tuning, total output power of 4.4 W and 35% PAE at 8 GHz has been achieved. However, typically gain compression was high, ranging from 4 to 7 dB, when the device reached its highest output power level, which was related to the immature material technology. This limited the large-signal gain and efficiency of the amplifiers. Nevertheless, in terms of realization of the high power potential of GaN, our “baseline” GaN-grown-on-sapphire power device process has been adequate for the subsequent design and fabrication of the power amplifiers.

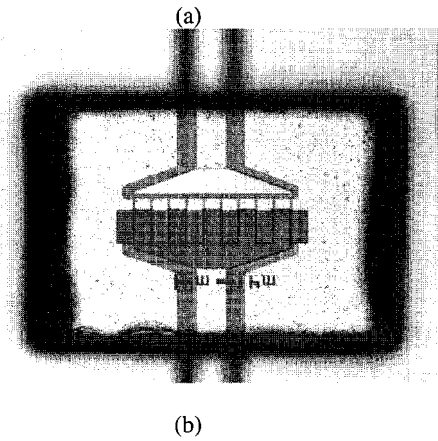
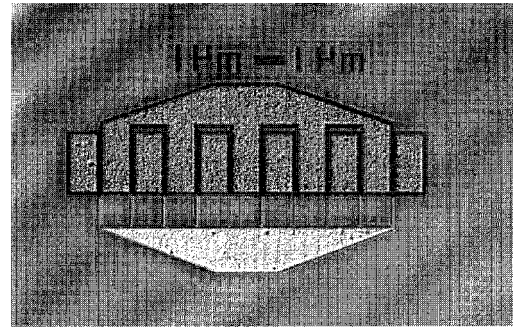


Fig. 3. Photograph of a 1-mm-wide GaN HEMT: (a) before bonding and (b) after bonding.

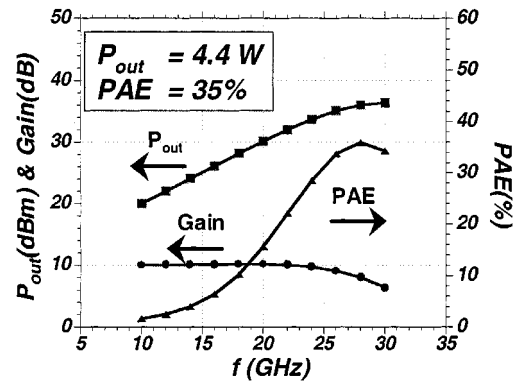


Fig. 4. Power performance of a 1-mm-wide GaN-HEMT-on-sapphire. ( $L_g = 0.7 \mu\text{m}$ ,  $W_g = 1 \text{ mm}$ ,  $f = 8 \text{ GHz}$ , biased at  $V_{\text{ds}} = 27 \text{ V}$ ,  $I_{\text{ds}} = 150 \text{ mA}$ , class AB mode.)

The device has characteristics of  $I_{\max} = 800 \text{ mA}$ ,  $g_{m\_intrinsic} = 320 \text{ mS}$ ,  $V_{\text{knee}} = 5 \text{ V}$ ,  $V_{\text{pinchoff}} = -4 \text{ V}$ , and  $V_{\text{breakdown}} = 40\text{--}50 \text{ V}$ . The current gain and power gain cutoff frequencies were about 20 and 40 GHz, respectively. The optimum load for the maximum output power of this 1-mm-wide 0.7- $\mu\text{m}$ -long device was  $R_{\text{opt}} = 30 \Omega$ ,  $C_{\text{ds}} = 0.3 \text{ pF}$ . Since accurate large-signal model is not available, the load-pull measurement of the optimum load is used for the design of the amplifier.

### III. AMPLIFIER DESIGN AND PERFORMANCE

Fig. 5 shows the small-signal model for a 1-mm-wide 0.7- $\mu\text{m}$ -long GaN HEMT used in this work. All model

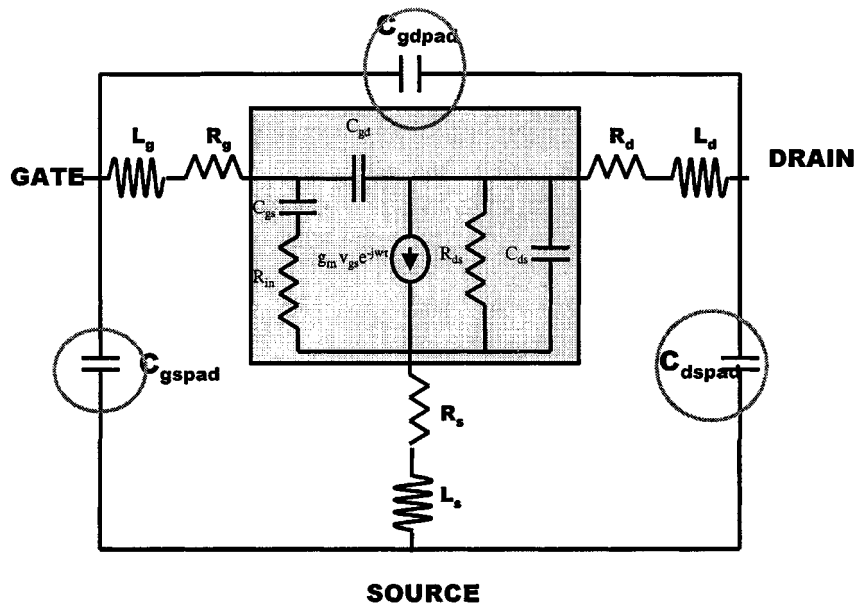


Fig. 5. Small-signal model for a 1-mm-wide, 0.7- $\mu$ m-long GaN/AlGaIn HEMT.

elements were extracted by  $S$ -parameter fitting. The parameters are  $C_{gs} = 2.5$  pF,  $C_{gd} = 0.015$  pF,  $C_{ds} = 0.015$  pF,  $R_g = 0.75$   $\Omega$ ,  $R_{in} = 1$   $\Omega$ ,  $R_s = 2$   $\Omega$ ,  $R_d = 2.5$   $\Omega$ ,  $R_{gd} = 10$   $\Omega$ ,  $R_{ds} = 150$   $\Omega$ ,  $C_{gs\ pad} = 0.15$  pF,  $C_{ds\ pad} = 0.25$  pF,  $C_{gd\ pad} = 0.15$  pF, and  $g_m = 0.32$  S. As can be seen, extra pad parasitic capacitances were added to the intrinsic elements (the shaded area) and the normal extrinsic parasitic elements due to the enlarged source and drain pads. The effective input capacitance (including  $C_{gs}$ ,  $C_{gs\ pad}$ ,  $C_{gd}$ , and  $C_{gd\ pad}$ ) is about 2.5–3 pF, and effective input resistance (including gate resistance  $R_g$ , channel resistance  $R_{in}$ , and source resistance  $R_s$ ) is on the order of several ohms ( $\approx 3$ –4  $\Omega$ ). The high input capacitance poses a challenge for input reactance absorption over a wide bandwidth. The low input resistance increases the impedance transformation ratio (about  $4 \times 50$   $\Omega$  to 3  $\Omega$ , since the amplifier in this work incorporated four 1-mm devices), which requires complex broad-band matching network design. At the output, first, resistance-level transformation of 200 to 30  $\Omega$  has to be performed, and then effective  $C_{ds}$  has to be absorbed to match each device to its optimum load for maximum power.

We have previously reported a modified traveling wave power amplifier (TWPA) [4], [5] for realization of a wideband power amplifier. This topology can achieve good input matching and gain flatness since it employs the input artificial transmission line technique of a conventional TWA to accommodate the large input capacitance of the GaN HEMTs. Higher efficiency was achieved as compared with a conventional TWA by replacing the output artificial drain line with a more efficient corporate combiner structure, thus eliminating the “backward” wave. Capacitive division was also used to extend the bandwidth. To obtain equal input drive for each device, the capacitances were varied to compensate for the loss along the input line. However, since such a loss is frequency dependent, a perfect compensation can be realized only at one frequency, which was chosen at the midband in our design. The uneven input drive will reduce

the efficiency of the circuit, especially at the higher frequency of the band, since the combiner was designed assuming four output signals of equal amplitude and phase. Also, the reliability of the circuit was decreased due to the fact that some devices tend to be overdriven before all devices reach saturation.

In this study, we circumvent this uneven drive problem of TWPA by employing a novel  $LCR$ -matched broad-band power amplifier. The circuit schematic is shown in Fig. 6. A multistage corporate power divider and combiner were employed at the input and output, respectively, to distribute and collect power from these devices. The combiner networks used multiple-stage quarterwave transformers to realize the desired bandwidth and impedance transformation ratios (the desired impedance levels are naturally different at input and output). Input and output  $LC$  match networks were then utilized to reactively compensate for  $C_{gs}$  and  $C_{ds}$  and provide additional impedance transformation. A lossy  $LCR$  network (similar to what was reported in [6] for a single-device amplifier) was used at the input of the device to achieve the desired gain flatness over the designed bandwidth.

Since the overall efficiency of the amplifier is given by

$$\begin{aligned} \eta &= \frac{P_{out} - P_{in}}{P_{DC}} \\ &= \frac{P_{out\ dev} \cdot \eta_{out} - P_{out\ dev} / (\eta_{in} \cdot G)}{P_{DC}} \\ &= \frac{P_{out\ dev}}{P_{DC}} \left( \eta_{out} - \frac{1}{\eta_{in} \cdot G} \right) \end{aligned}$$

where  $\eta_{in}$  and  $\eta_{out}$  is the combining efficiency of the input corporate power divider and output combiner, respectively,  $G$  is the gain of the device, and  $P_{out\ dev}$  is the output power right at the output of the device. This equation shows that the efficiency is directly proportional to  $\eta_{out}$  if  $G$  is large enough to offset the loss of the input matching networks. We used two sections of quarterwave transmission lines at the output to realize impedance transformation while keeping the conduction

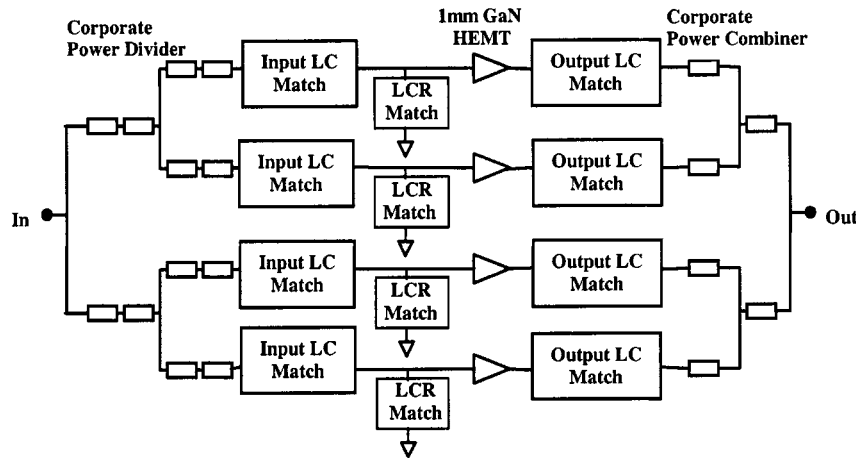


Fig. 6. Schematic of the 3–10-GHz *LCR*-matched GaN power amplifier.

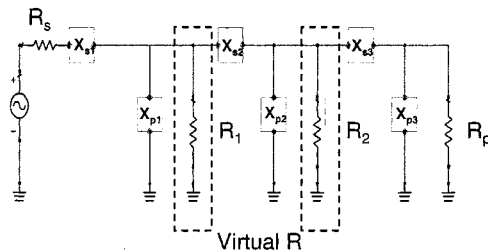


Fig. 7. Multisection *LC* matching networks.

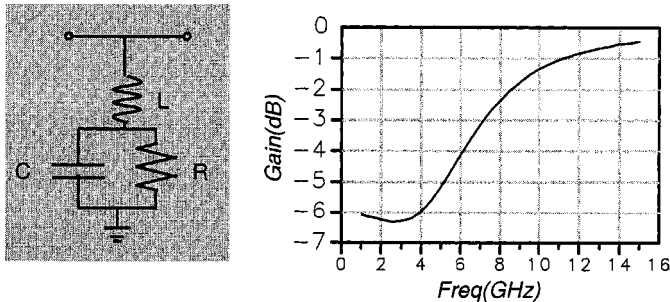


Fig. 8. *LCR* matching network and its frequency response ( $S_{21}$ ).

loss as low as possible. At the input, four sections of quarter-wave transmission lines need to be employed to be able to realize the high-ratio impedance transformation. The CPW transmission lines were meandered to reduce the circuit size.

Multisection low-pass *LC* networks were used at both the input and output of the device to absorb the reactance and provide additional impedance transformation (Fig. 7). We can extend the bandwidth by transforming resistance step by step, using virtual *R* as intervals for calculating values of *L* and *C* of each *LC* section. At the input of each device, a lossy *LCR* matching network was employed to provide the gain compensation and thus achieve the gain flatness over the whole bandwidth. Also, *R* served as a stabilizing resistor. Fig. 8 shows that the *LCR* matching network was aimed to eliminate gain peaks at low band and has little effect at high band. Its frequency response ( $S_{21}$ ) was plotted with parameter values of  $L = 0.9$  nH,  $C = 0.65$  pF, and  $R = 30$   $\Omega$ .

The circuit was designed to operate over a 3–11.5-GHz frequency range using HPEssof simulation, with small-signal gain  $S_{21}$  of 8 dB, input match  $S_{11}$  of  $-10$  dB, and output match  $S_{22}$  of  $-6$  dB. The GaN HEMTs used in this work were fabricated using Stepper lithography with a  $0.7$ - $\mu\text{m}$  gate length,  $75$ - $\mu\text{m}$  gate finger length, and  $50$ - $\mu\text{m}$  gate-to-gate spacing. Due to the relatively low  $f_{\text{max}}$  and high  $C_{\text{gs}}$  of these devices, it proved more challenging to achieve the desired low input reflection throughout the bandwidth with this reactively matched circuit topology as compared with the earlier TWPA design.

Fig. 9 shows the photo of the finished amplifier. The circuit dimension was  $12 \times 8$  mm<sup>2</sup>. Due to difficulties in flip-chip mounting a large-area HEMT's device, our design used two separate chips (each had two adjacent 1-mm devices) for a total of 4 mm of gate periphery. Fabricated on a 10-mil-thick polished AlN substrate ( $\epsilon_r = 8.5$ ), the circuit components include NiCr resistors, MIM capacitors using SiN as the insulating layer, air bridges, and two flipped 2-mm-wide GaN HEMTs chips. All the device and ceramic circuit processing was carried out at UCSB. Fig. 10 shows the small-signal performance of the circuit. The measured  $S_{21}$  was about 7 dB with 3-dB bandwidth of 3–10 GHz. We expect to extend the bandwidth to above 11 GHz by shrinking the gate length to  $0.6$   $\mu\text{m}$ . The measured  $S_{11}$  was less than  $-8$  dB, and  $S_{22}$  was less than  $-5$  dB over the band, which was expected, since output is not conjugated matched. Both were close to the simulation mentioned earlier.

Power measurement over the whole bandwidth is shown in Fig. 11. The highest power of 8 W (CW) was obtained at 9.5 GHz, and the lowest power of 4.5 W (CW) at 4.5 GHz was measured. The circuit was biased at 24 V,  $I_d = 500$  mA (about 15% of  $I_{\text{max}}$ ), in class AB mode. PAE ranged from 5% at 4.5 GHz to about 20% at 9.5 GHz. Although the PAE has been improved by about 5–10% compared with the previous TWPA, it was still about half of the expected value. The main reason was that the large-signal gain was only about 3–4 dB since the gain compression was almost 4 dB when devices were driven into saturation, as mentioned earlier, which causes much lower PAE than the drain efficiency. Nonuniformity of each device due to the nonuniformity of the wafer, the dc resistive loss in signal lines, and RF loss at corners of the meandering CPW lines may also contribute to the lowered PAE.

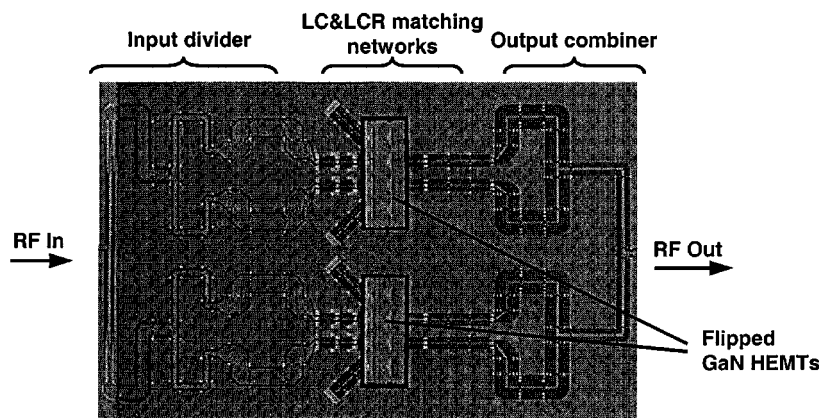


Fig. 9. Photograph of the fabricated *LCR*-matched amplifier.

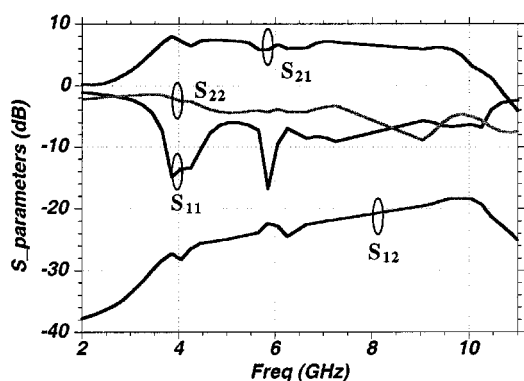


Fig. 10. Small-signal performance of the amplifier. (Biased at  $V_{ds} = 15$  V,  $I_{ds} = 500$  mA.)

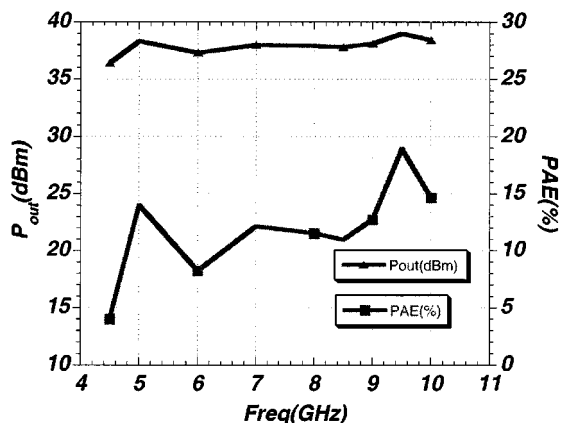


Fig. 11. Power measurement from 4.5 to 10 GHz. (Biased at  $V_{ds} = 24$  V,  $I_{ds} = 500$  mA.)

IV. CONCLUSION

We have successfully fabricated a second generation of GaN-based broad-band power amplifiers with advanced power performance. Compared with the first design of TWPA topology, *LCR*-matched circuit topology eliminates the problem of uneven input drive of the devices; the tradeoff is the increased input return loss and reduced gain flatness. The circuit had about 7 dB small-signal gain, with 3-dB bandwidth of 3–10 GHz. The input and output return loss was about 8 and 5 dB, respectively. At 9.5 GHz, *LCR*-matched PA was able to generate 8 W output

power with about 20% PAE using a total of 4-mm-wide devices resulting in 2-W/mm output power density. To our knowledge, this power level is the highest for a power amplifier using GaN-HEMTs-on-sapphire. Although lower than 4.4 W/mm results using 1-mm-wide devices, which is mainly due to the increased complexity in thermal management and matching network as the device size increases, this circuit has superior power performance in terms of power density than GaAs-based counterparts with the same size devices can achieve.

However, these initial demonstrations of GaN-based power amplifiers are still at a very early stage. The AlGaIn/GaN HEMTs material system is undergoing intensive investigation on certain key areas, such as wafer uniformity, trapping effect, high gain compression, etc., which may contribute to the low PAE (compared with its GaAs counterpart) and poor reliability of the fabricated circuits. Rapid progress is expected in the near future as GaN material and device technology matures.

ACKNOWLEDGMENT

The authors would like to thank Y.-F. Wu, Nitres Inc., Goleta, CA, for his valuable advice and insight.

REFERENCES

- [1] S. T. Sheppard, K. Doverspike, W. L. Pribble, S. T. Allen, J. W. Palmour, L. T. Kehias, and T. J. Jenkins, "High-power microwave GaN/AlGaIn HEMT's on semi-insulating silicon carbide substrates," *IEEE Electron Device Lett.*, vol. 20, pp. 161–163, Apr. 1999.
- [2] Y.-F. Wu, D. Kapolnek, J. Ibbetson, N.-Q. Zhang, P. Parikh, B. P. Keller, and U. K. Mishra, "High Al-content AlGaIn/GaN HEMT's on SiC substrates with very high power performance," in *Tech. Dig. Int. Electron Devices Meeting 1999*, Washington, DC, Dec. 5–8, 1999.
- [3] N.-Q. Zhang, S. Keller, L. McCarthy, S. P. DenBaars, and U. K. Mishra, "6.6-Watt/mm AlGaIn/GaN HEMT's on sapphire substrate," submitted for publication.
- [4] J. J. Xu, Y.-F. Wu, S. Keller, S. Heikman, B. J. Thibeault, U. K. Mishra, and R. A. York, "1-8-GHz GaN-based power amplifier using flip-chip bonding," *IEEE Microwave Guided Wave Lett.*, vol. 9, pp. 277–279, July 1999.
- [5] E. S. Shapiro, J. J. Xu, A. S. Nagra, F. Williams Jr., U. K. Mishra, and R. A. York, "A high-efficiency traveling-wave power amplifier topology using improved power-combining techniques," *IEEE Microwave Guided Wave Lett.*, vol. 8, pp. 133–135, Mar. 1998.
- [6] Y.-F. Wu, R. A. York, S. Keller, B. P. Keller, and U. K. Mishra, "3–9 GHz GaN-based microwave power amplifiers with *LCR* broad-band matching," *IEEE Microwave Guided Wave Lett.*, vol. 9, pp. 314–316, Aug. 1999.

**Jane J. Xu** was born in Shanghai, China. She received the B.S. and M.S. degrees in optical instrument engineering from Zhejiang University, Hangzhou, China, in 1992 and 1995, respectively. She is currently pursuing the Ph.D. degree in the Department of Electrical Engineering, University of California at Santa Barbara.

Her research interests are high-power GaN devices and GaN-based broad-band power amplifiers.

**Stacia Keller** received the diploma and the Ph.D. degrees in chemistry from the University of Leipzig, Germany, in 1983 and 1986, respectively.

As a Scientific Assistant, she continued her experimental and theoretical work in the field of epitaxial growth of GaAs- and InP-based semiconductors at the University of Leipzig. After joining the Electrical and Computer Engineering Department at the University of California, Santa Barbara, in 1994, her main research interests have been the crystal growth and characterization of group-III nitrides for electronic and optoelectronic applications. She has published more than 40 journal papers and more than 40 conference papers. She has received four patents.

**Gia Parish** was born in Perth, Australia. She received the B.S. degree in chemistry and the B.E. degree in electronic engineering from the University of Western Australia, Perth, in 1995 and the M.E.S. degree in electronic engineering from the University of Western Australia in 1997. She is pursuing the Ph.D. degree at the University of California, Santa Barbara.

Her research interests include growth of III-nitride epitaxial structures by metalorganic chemical vapor deposition for use in high electron mobility transistors and ultraviolet detectors, as well as in fabrication of ultraviolet detectors.

Ms. Parish is a member of the IEEE Electron Devices Society.

**Sten Heikman** received the M.S. degree in electrical engineering from the University of Massachusetts, Amherst, in 1998. He is currently pursuing the Ph.D. degree in electrical engineering at the University of California, Santa Barbara.

His research interests include high electron mobility transistors, device physics, processing technology, and epitaxial growth.

**Umesh K. Mishra** (S'80-M'83-SM'90-F95) received the Ph.D. degree from Cornell University, Ithaca NY, in 1984.

He worked in various laboratory and academic institutions, including Hughes Research Laboratories, Malibu, CA; the University of Michigan at Ann Arbor; and General Electric, Syracuse, NY, where he has made major contributions to the development of AlInAs-GaInAs HEMTs and HBTs. He is now a Professor in the Department of Electrical and Computer Engineering, University of California, Santa Barbara. His current research interests are in oxide-based III-V electronics and III-V nitride electronics and optoelectronics. He has published more than 120 papers in technical journals and conferences and has received five patents.

Mr. Mishra received the Hyland Patent Award from Hughes Aircraft and the Scientist of the Year Award from the International Symposium on GaAs and Related Compounds.

**Robert A. York** (S'85-M'89-SM'99) received the B.S. degree in electrical engineering from the University of New Hampshire, Durham, in 1987 and the M.S. and Ph.D. degrees in electrical engineering from Cornell University, Ithaca, NY, in 1989 and 1991, respectively.

He is currently an Associate Professor of electrical and computer engineering at the University of California, Santa Barbara (UCSB). His group at UCSB is currently involved with the design and fabrication of novel microwave and millimeter-wave circuits, microwave photonics, high-power microwave and millimeter-wave modules using spatial combining and wide-bandgap semiconductor devices, and application of ferroelectric materials to microwave and millimeter-wave circuits and systems.

Dr. York received the 1993 Army Research Office Young Investigator Award and the 1996 Office of Naval Research Young Investigator Award.